Sanchez-Marcos, J., Mazario, E., Rodriguez-Velamazan, J. A., Salas, E., Herrasti, P., & Menendez, N. (2018). Cation distribution of cobalt ferrite electrosynthesized nanoparticles. A methodological comparison. *In Journal of Alloys and Compounds, 739*, 909–917

DOI:10.1016/j.jallcom.2017.12.342

Cation distribution of Cobalt Ferrite Electrosynthesized Nanoparticles.

A methodological comparison.

J. Sanchez-Marcos[a], E. Mazario[a], J. A. Rodriguez-Velamazan[b], E. Salas[c], P. Herrasti[a], N. Menendez[a,*]

[a]Universidad Autónoma de Madrid, Facultad de Ciencias, Departamento de Química Física Aplicada. 28049 Madrid, Spain.

[b]Institut Laue Langevin, 6 rue Jules Horowitz, BP 156, F-38042 Grenoble. France

[c.]Spline Spanish CRG Beanline at European Synchrotron Radiation Facilities, ESRF-BP-220-38043 Grenoble Cedex, France

[*] Corresponding authors.

E-mail address: nieves.menendez@uam.es (N. Menendez)

Abstract

The present work seeks to analyse the structural and magnetic properties of cobalt ferrite nanoparticles obtained by electrochemical synthesis by high-resolution transmission electronic microscopy (HRTEM), X-ray absorption spectroscopy (XAS), Mössbauer spectroscopy (MS), neutron diffraction (ND) and SQUID magnetometer. The cationic distribution is analysed by different techniques. The inversion degree determined by the most accurate measurements was 0.73(1), and the formula for the nanoparticles therefore was $(\uparrow Co_{0.27}Fe_{0.73})[\downarrow Co_{0.73}Fe_{1.27}]O_4$. The magnetic moment found from DC and Mössbauer spectroscopy measurements was 3.8(3) µB, and the coercivity was 7870 Oe at 100 K.

1. Introduction

Recently, the study of nanoferrites has attracted great interest owing to their magnetic properties, such as superparamagnetism[1], spin canting[2,3], spin glass[4] or metamagnetism[5] that are different from those of bulk materials. Therefore, magnetic nanoparticles and especially ferrite nanoparticles are used in many applications, such as electronics[6], magnetic recording[7] permanent magnets[8,9] and biomedical industries[10,11]. Among the different ferrite materials, cobalt ferrite nanoparticles hold a special interest because of their high magnetocrystalline anisotropy, saturation magnetization, large magneto-optical coefficients, large coercive field and mechanical hardness[5].

The spinel cobalt ferrite structure is represented by the $(Co_{1-x}Fe_x)[Co_xFe_{2-x}]O_4$ formula, where round and square brackets represent the tetrahedral and octahedral sites, respectively. Magnetic properties of ferrite nanoparticles are directly related to the composition, particle size and cation distribution over the tetrahedral and octahedral lattice sites, while the coercive field also depends on the particle shape. Several recent studies have been also examined combinations of different metal cations with Co^{2+} in order to modulate the magnetic properties of the cobalt ferrite[12–15].

In a general view, the magnetic moments of the ions in the tetrahedral sites (M_t) are ordered parallel, and the same holds for the octahedral ions (M_o), while the two sublattices order antiparallel to each other. However, the existence of noncollinear spin structures associated with magnetic disorder at the nanoparticle surface has been confirmed in $CoFe_2O_4$[12,16,17]. The magnetic moment of the global ferrite is the difference between the moments of the two magnetic

sublattices (2 M_o-M_t), hence it is important to know the cation site distribution and the angular spin canting of each sublattice.

Various preparation techniques, such as hydrothermal synthesis[18], coprecipitation[19], sol-gel[20], polymer pyrolysis[21] and mechanical alloying[22] have been reported for producing cobalt ferrites. It has been found that cobalt ferrites of similar composition differ in their magnetic properties depending on the preparation technique, probably owing to different particle size and inversion degree (γ), which is the fraction of the iron atoms occupying tetrahedral sites. The inversion degree in ferrites with spinel structure mainly depends on the method of synthesis[23,24] and their thermal history[25]. Blanco-Gutierrez et al. obtained inversion degrees of 0.77 and 0.70 for cobalt ferrite particle sizes of 100 and 15 nm respectively, synthesized by the solvothermal method[26]. An inversion order of 0.72 and 0.70 were obtained by Peddis et al[23] and Mameli et al[13] respectively, for 6 nm cobalt ferrites synthesized by thermal decomposition. In this work, our goal has been to go deeper in the knowledge of the structural and magnetic properties of this electrosinthetized compound by different techniques with different experimental time windows and compare the results.

Owing to the difference by only one electron between Co and Fe, X-ray diffraction is not suitable for determining this cation distribution. In contrast, the neutron scattering factors are sufficiently different to distinguish between the Co and Fe atoms, making neutron diffraction (ND) analysis a good option. Furthermore, neutron diffraction provides a good sensitivity to oxygen, so that the stoichiometry of the samples could be studied. Therefore, ND was employed to determine the crystal and magnetic structure. The cation distribution was

analyzed by ND and ^{57}Fe Mössbauer spectroscopy because this technique is very effective in determining the environment of Fe ions. Finally, the cation oxidation state was studied by X-Ray absorption spectroscopy. The magnetic study of the material was also presented.

2. Experimental Methods

2.1 Electrochemical Synthesis

The details of the electrochemical synthesis procedure and characterization have been reported elsewhere[27,28]. Briefly, the electrosynthesis was carried out using two iron and cobalt foils as the anodes, and a cylindrical iron foil as the cathode. In this case the experimental parameters were tuned to obtain stoichiometric $CoFe_2O_4$ nanoparticles at 25 °C. The current densities of 40 mA cm^{-2} and 25 mA cm^{-2} were applied to the iron and cobalt anode electrodes, respectively. The electrosynthesis time was 30 minutes. The final product was washed several times by magnetic decantation with an aqueous solution of nitric acid at pH 3.2. ICP analysis, X-Ray diffraction and TEM microscopy were performed and corroborate the formation of an unique phase of stoichiometric $CoFe_2O_4$, with a mean diameter of 22 nm (σ=4). More details of the characterization were implemented in supporting information file.

2.1 Characterization Techniques

Spherical aberration (Cs)-corrected scanning transmission electron microscopy (STEM) was performed using a FEI Titan XFEG operated at 300 kV. The electron microscope was equipped with a CEOS corrector for the electron probe, allowing a spatial resolution of 0.8 Å. It was also fitted with a high-angle annular

dark-field (HAADF) detector, an EDAX EDS detector and a Gatan Tridiem energy filter for spectroscopic analyses.

To obtain information about the local coordination of spinel cations, the analysis of the X-ray absorption near-edge structure (XANES) and extended X-ray absorption fine structure (EXAFS) at the Co and Fe K-edges were performed in the transmission mode at the Spanish CRG beamline (SpLine, BM25 A) of the European Synchrotron Radiation Facility (ESRF). All spectra were obtained at room temperature and air atmosphere. The EXAFS analysis was performed using the Artemis programs[29]. The binding energy of all samples were determined in the maximum of the first derivate and the oscillations were obtained after removing the background with a cubic spline-fitting polynomial, and the EXAFS signal [$\chi(k)$] was obtained by normalizing the magnitude of the oscillations to the edge jump. The distribution functions around the cobalt and iron atoms was calculated by Fourier transformation of the k^3-weighted EXAFS signals [$k^3\chi(k)$].

The ^{57}Fe Mössbauer spectra were recorded using two ^{57}Co(Rh) γ-ray sources mounted on both ends of an electromagnetic transducer operated in the triangular mode. One of the sources was used for energy calibration with an α-Fe (6 μm) foil. The spectra were obtained between 4.2 and 300 K, in the presence and in the absence of an external magnetic field of 7 Tesla applied parallel to the γ-ray direction using an Oxford Spectromag 4000 M system. A MF-2A Ricor Ltd oven was used to obtain the Mössbauer spectra between 300 and 875 K. To avoid saturation effects and to optimize the signal-to-noise ratio, the sample thickness was 10 mg of natural Fe cm^{-2}. A boron nitride sample holder was used for high temperature measurements, while another sample holder with Be windows was used in the low-temperature range. The analysis of the spectra was performed

using the NORMOS program[30]. In all cases the isomer shifts (δ), and the hyperfine magnetic fields (H_{hf}) were refined; the quadrupole splitting values are near zero due to the cubic symmetry around the Fe nucleus.

The crystal and magnetic structure analysis was carried out using high-flux, D1B, and high-resolution, D2B, two-axis neutron powder diffractometers at ILL (Grenoble, France). Thermodiffractograms from room temperature up to 810 K, with the controlled heating rate of 2 K min^{-1}, were collected in D1B using the wavelength λ of 2.52 Å to determine the magnetic moment evolution with the temperature. Also, 100 K and 800 K patterns of 2 h were collected in D2B using the wavelength λ of 1.59 Å in order to study the cation distribution and the magnetic moment, which are compared with the Mössbauer results. Analysis of both the crystal structure and magnetic structure were performed with the FullProff suite package[31].

Magnetization data were obtained using a SQUID magnetometer (Quantum Design MPMS XL-5). The magnetization versus temperature curves were measured in zero-field-cooling (ZFC) and field-cooling (FC) procedures under different external applied magnetic field, H= 0.1, 0.5, 1, 5 and 10 kOe, and between 5 and 395 K. The magnetic hysteresis loops were obtained at 300, 200 and 100 K under a maximum applied magnetic field of 50 kOe.

3. Results and Discussion

3.1 High resolution Microscopy

Figures 1a and 1b show high-magnification HAADF-STEM images of some electrosynthesized nanoparticles in a diameter of 21-23 nm and "rounded"

morphology. Details of HAADF-STEM at atomic resolution reveal well-organized crystalline planes without domains (Figure 1c).

Electron Energy Loss Spectroscopy (EELS) was performed to corroborate the nanoparticle composition and the distribution of the elements along the nanoparticle surface. The compositional map of the extracted signals is described below. Oxygen is in red (Figure 1d), iron in green (Figure 1e), and cobalt in blue (Figure 1f). These images confirm that the nanoparticles consist of Fe, Co and O ions uniformly distributed over all nanoparticles, which present good crystallographic order.

3.2 XAS

Cobalt and iron K-edge X-ray Absorption Near-Edge Structure (XANES) spectra of $CoFe_2O_4$ nanoparticles are shown in Figure 2. For comparison, in the Co K-Edge spectra, Figure 2a, Co-foil, CoO and Co_3O_4 spectra with 0, +2 and (+2 and +3) oxidation states respectively have been included.

As can be seen in Figure 2a the Co K-Edge spectra of $CoFe_2O_4$ shows the typical white line observed in oxides and a binding energy at 7718 eV. Co foil, CoO and Co_3O_4 show the binding energies at 7700, 7718 and 7724 eV, respectively. This energy is related to the oxidation state, so that the cobalt atoms in the $CoFe_2O_4$ sample appear to be in the +2 oxidation state. Additionally, the spectra show a low intensity pre-edge feature at 7707 eV (inset Figure 2a), corresponding to the 1s→3d electronic transitions. This pre-edge feature is several times more intense for non-centrosymmetric tetrahedral environments than for the centrosymmetric octahedral site[32,33]. Comparison to the reference compounds shows that there is a similar low intensity of the pre-edge peak in $CoFe_2O_4$ and CoO. Moreover, the features observed above the binding energy in both compounds are very

similar, with a small shoulder around 7728 eV and a maximum at 7738 eV. These facts indicate that the Co in the $CoFe_2O_4$ samples exhibit very similar environments to that of Co in CoO, implying that Co is preferably located in the octahedral sites.

Regarding the iron K-edge spectra (Figure 2b), Fe foil, FeO, γ-Fe_2O_3 and Fe_3O_4 with 0, +2, +3 and (+2 and +3) oxidation states respectively have also been included. The $CoFe_2O_4$ sample shows a pre-edge peak or shoulder around 7110 eV followed by a rapid increase of the absorption up to the maximum at 7129 eV and with the binding energy of 7123 eV. On the other hand, Fe-foil, FeO, Fe_3O_4 and γ-Fe_2O_3 show the binding energies of 7116, 7118, 7120 and 7123 eV, respectively. The greatest similarity is observed between our sample and the γ-Fe_2O_3 binding energy, indicating the +3 oxidation state for Fe into $CoFe_2O_4$.

Inset of Figure 2b shows the different intensity of the pre-edge peak. At first sight, the ferrite peak is smaller than those of Fe_3O_4 and γ-Fe_2O_3 and larger than that of FeO, but taking the background into account, due to the edge, the intensity of ferrite is only slightly smaller than those for Fe_3O_4 and γ-Fe_2O_3, indicating that a large fraction of tetrahedral sites are occupied by iron cations. A rough estimation shows that, considering that the contribution of the octahedral sites to the pre-edge peak is negligible, 79% of the tetrahedral sites are occupied by iron (γ=0.79), so that Co atoms preferably but not only occupied the octahedral sites.

Extended X-ray absorption fine structure (EXAFS) was used to evaluate the crystallographic composition of the nanoparticles. Figure 3 shows the k^3-weighted Fourier transform (FT) magnitude obtained for the Co-ferrite compared to those for the Co and Fe oxides. Fourier transforms have been obtained within

the same k-range (3–10 Å^{-1}). As can be seen, the first coordination shell of Co ferrite, around 1.55 Å, (Figure 3a), is very similar to the results for CoO, whereas the second and higher coordination shells are more similar to those of Co_3O_4. That means that the environment of cobalt atoms is similar to the octahedral environment found in the CoO compound, but the overall structure is more similar to the one of Co_3O_4, which has the same spinel structure as the ferrites.

On the other hand, the first coordination shell of Fe in Co-ferrite (Figure 3b), is very similar to the γ-Fe_2O_3 result, whereas the second and further coordination shells look like Fe_3O_4. γ-Fe_2O_3 has a spinel structure but with iron vacancies at the octahedral sites, so that from the point of view of iron, the situation is the same in the Co ferrite; the iron in octahedral sites is lacking, so the Co cations are preferentially occupying the octahedral sites. However, the Fourier transform at larger distances (R) shows a Fe_3O_4 spinel structure.

3.3 Mössbauer Spectroscopy

For an in depth study of the spinel inversion of the ferrite, Mössbauer spectra were recorded from 4.2K to the paramagnetic region. As shown in Figure 4, which displays the most significant spectra, at temperatures above the magnetic order temperature, T_c, the spectra are fitted as two independent single lines within different intensities in agreement with their cubic structure. The most abundant component shows an isomer shift (δ) of 0.107(1) mm s^{-1} at 875 K, while the second single line shows a δ of -0.153(1) mm s^{-1}. If we consider that the isomer shift is increased by the temperature effect (second-order Doppler shift), these values correspond to the Fe^{3+} at the octahedral and tetrahedral spinel positions, respectively, and exclude the presence of Fe^{2+} in the material, in agreement with the XANES results. Assuming that the Lamb-Mössbauer factor is the same for

the ^{57}Fe in both positions, the subspectra area (A) show that 37% of Fe are in the tetrahedral position (A$_t$) and that 63% of Fe occupy the octahedral position (A$_o$), indicating the inversion degree γ =0.74. Below T$_c$ it is possible to obtain a reasonable fit of the spectra as the sum of two sextets corresponding to Fe^{3+} at the tetrahedral or octahedral sites, respectively. The hyperfine magnetic fields in both positions increase as the temperature decreases to practically reach the saturation at 4.2 K (see Figure 5). Nevertheless the relative resonant area of each subspectrum does not appear to be constant with temperature, although cation migration is discarded because the CoFe$_2$O$_4$ melting temperature is 1843 K[34]. The difficulty in obtaining the relative areas is because the subspectra overlap and therefore are resolved in energy only at very low temperatures. As shown in the literature[15,35], the linewidths of the sextet corresponding to the octahedral site are greater due to the different combinations of Fe^{3+} and Co^{2+} located at the tetrahedral position of the structure, (6Fe^{3+}, 5Fe^{3+} 1Co^{2+}, 4Fe^{3+} 2Co^{2+}....) and this line broadening generally leads to the under-estimation of the amount of Fe in the octahedral position. A more realistic areas ratio (α=A$_t$/A$_o$) is obtained considering that the subspectrum of Fe in the octahedral position is the result of the convolution of four sextets, in this case, corresponding to the four combinations of most probable neighbours. These probabilities are 0.16, 0.35, 0.30 and 0.14 as calculated from equation 1, using the inversion degree, γ=0.74 deduced from the 875 K subspectrum areas ratio (α) according to

$$I(n) = \binom{6}{n}(1-\gamma)^{6-n}\gamma^n \qquad\qquad (1)$$

where I(n) is the intensity of the octahedral sextet with nFe^{3+} cations in the tetrahedral site, $\gamma = (1\text{-}x)$ and $x = (1\text{-}\alpha)/(1\text{+}\alpha)$.

The CoFe$_2$O$_4$ spectra fitted assuming this model are shown in the Figure 4c and Figure 4d. In these cases, the fit below room temperature, was done with the constraints of equal linewidth of Fe$^{3+}_o$ sextets, intensities in the ratio 3:2:1:1:2:3 for the six peaks of each sextet and relative areas proportional to the calculated probabilities of the most probable neighbours in the tetrahedral site. The obtained hyperfine parameters are listed in Table 1, and show that for one Co^{2+} replacing one Fe^{3+} in the tetrahedral site, the hyperfine magnetic field in the octahedral position decreases by about 2 T, as reported at room temperature[17], whereas at 4.2 K the H$_{hf}$ for Fe$^{3+}_o$ decreases less than 1 T since the magnetic moments are near saturation.

Figure 5 shows the temperature evolution of the hyperfine magnetic field of the Fe nucleus in tetrahedral and octahedral sites and their fits to the equation 2

$$H(T) = BH_0 t_{red}^{\beta}\left[1 + At_{red}^{\Delta} + Ot_{red}^{2\Delta}\right] \qquad (2)$$

where t$_{red}$ is the reduced temperature of the system (t$_{red}$ = 1-T/T$_C$), β is the critical exponent of the paramagnetic-ferromagnetic phase transition, Δ is the correction to the scaling exponent of the transition, H$_0$ is the hyperfine magnetic field at 0 K and B, A and O are the material-dependent fitting parameters. To parameterize the evolution of the hyperfine fields, we have taken the theoretical values of critical parameters for a second-order phase transition in a three-dimensional Heisenberg ferromagnet, β = 0.365 and Δ = 0.550[36] obtaining 860 K as the T$_C$. At temperatures sufficiently below T$_C$, the values of δ and H$_{hf}$ are higher for the Fe^{3+} in the octahedral site than in the tetrahedral site owing to the more covalent character of the Fe$_t^{3+}$ - O^{2-} bond than the Fe$_o^{3+}$ - O^{2-} bond. Consequently, the s-electron density in the Fe$_t^{3+}$ nucleus is larger and therefore its isomer shift is

lower. Moreover, the covalence produces a positive contribution to the Fermi contact interaction, reducing the resulting hyperfine field. The crossing of the tetrahedral and octahedral H_{hf} at $T/T_C \approx 0.4$ is not common, but has been observed previously in $CoFe_2O_4$[37] and in other ferrites such as $MnFe_2O_4$[35], and is related to an "accidental" cation distribution in the spinel and their exchange strengths.

To break up the overlap of the sextets and to explore the possible spin canting at the surface, the spectra at different temperatures were also recorded by applying a 7 T external magnetic field (H_{ext}) parallel to the γ-ray direction (Figure 4e and 4f). The H_{ext} tends to align the magnetic moments along the field direction, and as the sublattice with the largest magnetic moment, the octahedral site, is aligned parallel to the applied field and antiparallel to the other site, so that the effective fields ($H_{eff} = H_{ext} + H_{hf}$) measured by Mössbauer spectroscopy are not overlapping, facilitating the spectra analysis.

Moreover, by applying a strong enough H_{ext} parallel to the γ-ray direction, the transitions with $\Delta m_I = 0$ (lines 2 and 5 of the sextet) disappear. However as seen in Figure 4, 7 T is not sufficient to overcome the magnetic anisotropy of the material, so in the fitting of the spectra the ratio of intensities of the spectral lines is set as 3:p:1:1:p:3, where p is given by equation 3.

$$p = \frac{4\sin^2\theta}{1+\cos^2\theta} \qquad\qquad (3)$$

where θ is the angle between the incident radiation and the effective field at each lattice position. Table 2 shows the Mössbauer parameter obtained taking into account the vector sum of the hyperfine fields and the applied field.

As shown in Table 2, the subspectra area ratio α is nearly constant with temperature as expected, and is in very good agreement with the cation distribution determined in the paramagnetic region. Thus, taking the area ratio from the spectrum at 4.2 K and H_{ext}= 7 T, we determine the inversion degree as γ=0.72 and therefore the stoichiometry of the ferrite as $(\uparrow Co_{0.28}Fe_{0.72})$ $[\downarrow Co_{0.72}Fe_{1.28}]_4$. The average spin canting shown by Fe at tetrahedral and octahedral positions (Table 2) is in agreement with the previously reported results[38] and is negligible for the Co atoms owing the high anisotropy energy[39]. From these spin canting values it is possible to calculate the effective magnetic moment of the ferrite as 3.4(3) μ_B at 4.2 K, where M_o= 3.8 (1) μ_B and M_t= 4.2(1)μ_B.

3.4 Neutron Diffraction

With the aim of obtaining deeper insight into the magnetic structure of $CoFe_2O_4$, a neutron diffraction study was carried out. Figure 6 shows the thermodiffractograms obtained between 430 and 810 K at the high flux D1B diffractometer. This figure shows the reflections related to the crystal spinel and magnetic structures in the whole temperature range.

As temperature increases, we observe a decrease in the background, probably related with the evaporation of surfactant molecules. A marked reduction of the intensity of some reflections is observed when the temperature increases up to ca. 800 K. No further significant changes occur above this temperature, indicating that the paramagnetic state is reached. The difference between this temperature and the T_C obtained by Mössbauer spectroscopy is due to the higher sensitivity of this last technique to small magnetic interactions.

A high resolution neutron diffraction pattern was collected at 800 K in the high-resolution D2B diffractometer (Figure 7a). All the observed peaks correspond to the Fd-3m (227) crystal structure reflections and no signature of other structure is identified. The atomic positions of cations are [8a, (1/8,1/8,1/8)] and [16d,(1/2,1/2,1/2)] whereas the oxygen position is [32e,(x,x,x)]. The analysis of the results shows that no significant oxygen vacancies are observed. The cobalt occupation obtained in the refinement (Table 3) allow us to calculate the inversion degree as 0.73, in agreement with the values obtained by Mössbauer spectroscopy (γ =0.74 at 875 K and γ =0.72 at 4.2 K).

The neutron diffraction pattern collected at 100 K is depicted in Figure 7b. As can be seen, no new peaks are observed, and only some reflection intensities increase. The (1 1 1) reflection at 18.96º 2θ shows the highest increase. The absence of new reflections indicates that the magnetic structure is described by a propagation vector k = (0,0,0), that is, the magnetic unit cell is the same that the crystal one.

Table 3 summarizes the refinement parameters of the magnetic phase, where we have fixed the cation distribution obtained at 800 K and the oxygen coordinates. The Debye-Waller factor is obtained at high angle, where the magnetic contribution is negligible. The total magnetic moment calculated at 100K from the magnetic moment shown in Table 3, is 2.5(1) μ_B. As usually happens with the magnetic moments determined by neutron diffraction, the values are lower than the ones obtained by in-field techniques. This fact is commonly attributed to an incomplete magnetic polarization in zero-field conditions and to a possible spin delocalization to the non-magnetic atoms surrounding the magnetic ions.

From the thermodiffractogram and structural data we can determine the magnetic moment evolution of both the octahedral and tetrahedral sites between 100 and 800 K. The resulting values are plotted in Figure 8. The thermal evolution of the magnetic moments shows a constant value below room temperature followed by a significant decrease with the temperature at approximately 600 K, in agreement with the previously mentioned intensity drop of the magnetic peaks and corresponding to a magnetic ordering phase transition. However, owing to the antiferromagentic alignment of both magnetic sites, the total magnetic moment (black line in Figure 7) shows a near zero value already around 650 K.

Finally, the ZFC and FC magnetization curves, from 5 to 395 K, at several external magnetic fields are depicted in Figure 9a. The FC curves show a nearly constant value of magnetization that decreases at high temperature and high magnetic fields, whereas the ZFC curves show a high irreversibility that decreases with the field. This behaviour is related to ferro- and ferrimagnetic materials at the nanoscale with the magnetic order temperature above 400 K. All curves show similar behaviour with a maximum in the ZFC curve at T_B. For 0.5 and 0.1 kOe the maximum is expected to be above 395 K. The T_B temperature is related to the freezing or blocking process of the nanoparticle magnetic moment. Additionally, a nearly constant value of FC below the blocking temperature is observed. Both behaviours are in agreement with the presence of the nanoparticles and with a high dipolar interparticle interaction[40]. As can be seen, the blocking temperature decreases with the external magnetic field, shifting from above 400 K for 1 kOe to 237 K for 10 kOe. The evolution of T_B with the magnetic field is related to the strong exchange interaction between the particles that allows a low-temperature order[41].

Figure 9b shows the hysteresis loops, M(H), and the initial magnetization curve of $CoFe_2O_4$ measured up to 50 kOe at 100, 200 and 300 K. At these three temperatures, a clear hysteresis appears with the coercivity field that decreases from 7.87 kOe at 100 K to 1.12 kOe at 300 K, in good agreement with previous works[17,42]. Also, a small decrease of saturation magnetization (M_S) is detected as temperature increases. Taking the drastic decrease of coercivity into account, it can be seen that the Co-ferrite nanoparticles show a clear ferromagnetic behaviour that is not far away from the superparamagnetic state.

To calculate M_S and the anisotropy constant (K), the high magnetic field region of the initial magnetization curve was fitted to the following approach law[43]

$$M(T) = M_S(T)\left(1 - \frac{a}{H} - \frac{b}{H^2}\right) \qquad (4)$$

where H is the magnetic field and b takes the value 0.076 K^2 M_S^{-2}, assuming single domain nanoparticles and independent grains. The last term of the equation is associated with the susceptibility at high field and could be correlated with the crystalline anisotropy constant, K. The values obtained for M_S and K at the three different measured temperatures are collected in Table 4. The magnetic moment calculated from the magnetization results are in agreement with the calculated values from Mössbauer spectroscopy results (3.5(3) μ_B at 100 K). The anisotropy values are higher than the corresponding cobalt ferrite bulk value $K = 2.10^5$ J m^{-3} at 298 K[44], which is related to surface effects or the surface anisotropy contribution. The obtained K values are comparable to other K values in the literature[45,46].

4. Conclusions

The cation distribution and magnetic properties of electrosynthetized cobalt ferrite nanoparticles have been studied by means of X-Ray Absortion and Mössbauer spectroscopy, DC magnetic measurements and neutron diffraction experiments.

$CoFe_2O_4$ particles obtained are nanometric (22(1) nm), well crystallized and exhibit a uniform distribution of the different atoms as shown by the HRTEM measurements. Cobalt and iron cation have a +2 and +3 oxidation state respectively confirmed by XAS and Mössbauer measurements.

All tested techniques show that Co atoms prefer the octahedral sites against tetrahedral one. The most accurate measurements, neutron diffraction and Mössbauer spectroscopy under an external magnet field, display a percentage of 36% of iron atoms in the tetrahedral site, leading to an inversion degree of γ=0.73(1). An approximate calculation from the XANES spectra allows obtaining the ferrite inversion degree with an error lower than 10%. On the other hand, although different techniques were used to obtain the ions position, it can also be concluded that the Mössbauer spectrum at high temperature give the same information taking into account the experimental error.

From de magnetic point of view, Mössbauer spectroscopy and magnetic susceptibility analysis are in agreement with a value of 3.8(3) μB per unit formula at 100 K, whereas ND confirms the ferrimagnetic structure. The low magnetic moment obtained in ND comparing to the other techniques is associated with the absence of external magnetic field during the measurements.

Acknowledgements

References

[1]   C. Liu, B. Zou, A.J. Rondinone, Z.J. Zhang, Chemical control of superparamagnetic properties of magnesium and cobalt spinel ferrite nanoparticles through atomic level magnetic couplings, J. Am. Chem. Soc. 122 (2000) 6263–6267. doi:10.1021/ja000784g.

[2]   S.J. Stewart, R.C. Mercader, R.E. Vandenberghe, G. Cernicchiaro, R.B. Scorzelli, Magnetic anomalies and canting effects in nanocrystalline spinel copper ferrites CuxFe3-xO4, J. Appl. Phys. 97 (2005). doi:10.1063/1.1852095.

[3]   A.T. Ngo, P. Bonville, M.P. Pileni, Spin canting and size effects in nanoparticles of nonstoichiometric cobalt ferrite, J. Appl. Phys. 89 (2001) 3370–3376. doi:10.1063/1.1347001.

[4]   R.H. Kodama, A.E. Berkowitz, E.J. McNiff, S. Foner, Surface spin disorder in ferrite nanoparticles (invited), J. Appl. Phys. 81 (1997) 5552. doi:10.1063/1.364659.

[5]   S. Rani, Y. Sharma, G.D. Varma, Structurally Induced Spin Canting and Metamagnetism in CoFe2O4 Nanoparticles Synthesized via Co-precipitation

Method, J. Supercond. Nov. Magn. 28 (2015) 3633–3644. doi:10.1007/s10948-015-3205-4.

[6]   D.M. Jnaneshwara, D.N. Avadhani, B. Daruka Prasad, B.M. Nagabhushana, H. Nagabhushana, S.C. Sharma, S.C. Prashantha, C. Shivakumara, Effect of zinc substitution on the nanocobalt ferrite powders for nanoelectronic devices, J. Alloys Compd. 587 (2014) 50–58. doi:10.1016/j.jallcom.2013.10.146.

[7]   R. Rani, S.K. Sharma, K.R. Pirota, M. Knobel, S. Thakur, M. Singh, Effect of zinc concentration on the magnetic properties of cobalt-zinc nanoferrite, Ceram. Int. 38 (2012) 2389–2394. doi:10.1016/j.ceramint.2011.11.004.

[8]   A. López-Ortega, E. Lottini, C.D.J. Fernández, C. Sangregorio, Exploring the Magnetic Properties of Cobalt-Ferrite Nanoparticles for the Development of a Rare-Earth-Free Permanent Magnet, Chem. Mater. 27 (2015) 4048–4056. doi:10.1021/acs.chemmater.5b01034.

[9]   F.J. Pedrosa, J. Rial, K.M. Golasinski, M.N. Guzik, A. Quesada, J.F. Fernández, S. Deledda, J. Camarero, A. Bollero, Towards high performance $CoFe_2O_4$ isotropic nanocrystalline powder for permanent magnet applications, Appl. Phys. Lett. 109 (2016) 223105. doi:10.1063/1.4969064.

[10]   G.A.O. Jinhao, G.U. Hongwei, X.U. Bing, Multifunctional magnetic nanoparticles: design, synthesis, and biomedical applications, Acc. Chem. Res. 42 (2009) 1097–1107. doi:10.1021/ar9000026.

[11]   A.K. Gupta, M. Gupta, Synthesis and surface engineering of iron oxide nanoparticles for biomedical applications, Biomaterials. 26 (2005) 3995–4021. doi:10.1016/j.biomaterials.2004.10.012.

[12]   G. Muscas, N. Yaacoub, G. Concas, F. Sayed, R. Sayed Hassan, J.M. Greneche, C. Cannas, A. Musinu, V. Foglietti, S. Casciardi, C. Sangregorio, D. Peddis,

Evolution of the magnetic structure with chemical composition in spinel iron oxide nanoparticles, Nanoscale. 7 (2015) 13576–13585. doi:10.1039/C5NR02723C.

[13] V. Mameli, A. Musinu, A. Ardu, G. Ennas, D. Peddis, D. Niznansky, C. Sangregorio, C. Innocenti, N.T.K. Thanh, C. Cannas, Studying the effect of Zn-substitution on the magnetic and hyperthermic properties of cobalt ferrite nanoparticles, Nanoscale. 8 (2016) 10124–10137. doi:10.1039/C6NR01303A.

[14] R.K. Panda, R. Muduli, G. Jayarao, D. Sanyal, D. Behera, Effect of Cr3+ substitution on electric and magnetic properties of cobalt ferrite nanoparticles, J. Alloys Compd. 669 (2016) 19–28. doi:10.1016/j.jallcom.2016.01.256.

[15] M. Atif, M. Idrees, M. Nadeem, M. Siddique, M.W. Ashraf, Investigation on the structural, dielectric and impedance analysis of manganese substituted cobalt ferrite i.e., Co1−xMnxFe2O4 ($0.0 \leq x \leq 0.4$), RSC Adv. 6 (2016) 20876–20885. doi:10.1039/C5RA20621A.

[16] D. Peddis, M. V. Mansilla, S. Mørup, C. Cannas, A. Musinu, G. Piccaluga, F. D'Orazio, F. Lucari, D. Fiorani, F. D'Orazio, F. Lucari, D. Fiorani, F. D'Orazio, F. Lucari, D. Fiorani, Spin-Canting and Magnetic Anisotropy in Ultrasmall CoFe2O4 Nanoparticles, J. Phys. Chem. B. 112 (2008) 8507–8513. doi:10.1021/jp8016634.

[17] S.R. Naik, A. V. Salker, S.M. Yusuf, S.S. Meena, Influence of Co2+ distribution and spin-orbit coupling on the resultant magnetic properties of spinel cobalt ferrite nanocrystals, J. Alloys Compd. 566 (2013) 54–61. doi:10.1016/j.jallcom.2013.02.163.

[18] M.P. Reddy, A. Mohamed, X. Zhou, S. Du, Q. Huang, A facile hydrothermal synthesis, characterization and magnetic properties of mesoporous CoFe2O4

nanospheres, J. Magn. Magn. Mater. 388 (2015) 40–44. doi:10.1016/j.jmmm.2015.04.009.

[19] Y.M. Abbas, S.A. Mansour, M.H. Ibrahim, S.E. Ali, Microstructure characterization and cation distribution of nanocrystalline cobalt ferrite, J. Magn. Magn. Mater. 323 (2011) 2748–2756. doi:10.1016/j.jmmm.2011.05.038.

[20] M. Sajjia, M. Oubaha, M. Hasanuzzaman, A.G. Olabi, Developments of cobalt ferrite nanoparticles prepared by the sol-gel process, Ceram. Int. 40 (2014) 1147–1154. doi:10.1016/j.ceramint.2013.06.116.

[21] E. Swatsitang, S. Phokha, S. Hunpratub, B. Usher, A. Bootchanont, S. Maensiri, P. Chindaprasirt, Characterization and magnetic properties of cobalt ferrite nanoparticles, J. Alloys Compd. 664 (2016) 792–797. doi:10.1016/j.jallcom.2015.12.230.

[22] C. Behera, R.N.P. Choudhary, P.R. Das, Size effect on electrical and magnetic properties of mechanically alloyed $CoFe_2O_4$ nanoferrite, J. Mater. Sci. Mater. Electron. 26 (2015) 2343–2356. doi:10.1007/s10854-015-2690-3.

[23] D. Peddis, N. Yaacoub, M. Ferretti, A. Martinelli, G. Piccaluga, A. Musinu, C. Cannas, G. Navarra, J.M. Greneche, D. Fiorani, Cationic distribution and spin canting in $CoFe_2O_4$ nanoparticles, J. Phys. Condens. Matter. 23 (2011) 426004. doi:10.1088/0953-8984/23/42/426004.

[24] H. Le Trong, L. Presmanes, E. De Grave, A. Barnabé, C. Bonningue, P. Tailhades, Mössbauer characterisations and magnetic properties of iron cobaltites $Co_xFe_{3-x}O_4$ ($1 \leq x \leq 2.46$) before and after spinodal decomposition, J. Magn. Magn. Mater. 334 (2013) 66–73. doi:10.1016/j.jmmm.2013.01.007.

[25] G.A. Sawatzky, F. Van Der Woude, A.H. Morrish, Cation distributions in octahedral and tetrahedral sites of the ferrimagnetic spinel $CoFe_2O_4$, J. Appl.

Phys. 39 (1968) 1204–1205. doi:10.1063/1.1656224.

[26] V. Blanco-Gutiérrez, J.A. Gallastegui, P. Bonville, M.J. Torralvo-Fernández, R. Sáez-Puche, MFe2O4 (M: Co2+, Ni2+) nanoparticles: Mössbauer and X-ray absorption spectroscopies studies and high-temperature superparamagnetic behavior, J. Phys. Chem. C. 116 (2012) 24331–24339. doi:10.1021/jp307371q.

[27] E. Mazarío, P. Herrasti, M.P. Morales, N. Menéndez, Synthesis and characterization of CoFe2O4 ferrite nanoparticles obtained by an electrochemical method, Nanotechnology. 23 (2012) 355708. doi:10.1088/0957-4484/23/35/355708.

[28] E. Mazario, N. Menéndez, P. Herrasti, M. Cañete, V. Connord, J. Carrey, Magnetic Hyperthermia Properties of Electrosynthesized Cobalt Ferrite Nanoparticles, J. Phys. Chem. C. 117 (2013) 11405–11411. doi:10.1021/jp4023025.

[29] B. Ravel, M. Newville, ATHENA , ARTEMIS , HEPHAESTUS : data analysis for X-ray absorption spectroscopy using IFEFFIT, J. Synchrotron Radiat. 12 (2005) 537–541. doi:10.1107/S0909049505012719.

[30] R.A. Brand, Improving the validity of hyperfine field distributions from magnetic alloys, Nucl. Instruments Methods Phys. Res. Sect. B Beam Interact. with Mater. Atoms. 28 (1987) 398–416. doi:10.1016/0168-583X(87)90182-0.

[31] J. Rodríguez-Carvajal, Recent advances in magnetic structure determination by neutron powder diffraction, Phys. B Condens. Matter. 192 (1993) 55–69. doi:10.1016/0921-4526(93)90108-I.

[32] D. Carta, M.F. Casula, A. Falqui, D. Loche, G. Mountjoy, C. Sangregorio, A. Corrias, A Structural and Magnetic Investigation of the Inversion Degree in Ferrite Nanocrystals MFe2O4 (M = Mn, Co, Ni), J. Phys. Chem. C. 113 (2009)

8606–8615. doi:10.1021/jp901077c.

[33] M.H. Nilsen, C. Nordhei, A.L. Ramstad, D.G. Nicholson, M. Poliakoff, A.

Cabañas, XAS (XANES and EXAFS) investigations of nanoparticulate ferrites

synthesized continuously in near critical and supercritical water, J. Phys. Chem.

C. 111 (2007) 6252–6262. doi:10.1021/jp0626723.

[34] A. Goldman, Modern Ferrite Technology, Springer US, 2006. doi:10.1007/978-

0-387-29413-1.

[35] G.A. Sawatzky, F. Van Der Woude, A.H. Morrish, Mössbauer Study of Several

Ferrimagnetic Spinels, Phys. Rev. 187 (1969) 747–757.

doi:10.1103/PhysRev.187.747.

[36] H. Keller, I.M. Savić, Mössbauer studies of the static and dynamic critical

behavior of the layered antiferromagnets RbFeF4 and KFeF4, Phys. Rev. B. 28

(1983) 2638–2652. doi:10.1103/PhysRevB.28.2638.

[37] G.A. Sawatzky, F. Van Der Woude, A.H. Morrish, Cation Distributions in

Octahedral and Tetrahedral Sites of the Ferrimagnetic Spinel CoFe2O4, J. Appl.

Phys. 39 (1968) 1204–1205. doi:10.1063/1.1656224.

[38] D. Peddis, N. Yaacoub, M. Ferretti, A. Martinelli, G. Piccaluga, A. Musinu, C.

Cannas, G. Navarra, J.M. Greneche, D. Fiorani, Cationic distribution and spin

canting in CoFe2O4 nanoparticles, J. Phys. Condens. Matter. 23 (2011) 426004.

doi:10.1088/0953-8984/23/42/426004.

[39] C. Cannas, A. Musinu, G. Piccaluga, D. Fiorani, D. Peddis, H.K. Rasmussen, S.

Mørup, Magnetic properties of cobalt ferrite–silica nanocomposites prepared by a

sol-gel autocombustion technique, J. Chem. Phys. 125 (2006) 164714.

doi:10.1063/1.2354475.

[40] E. De Biasi, R.D. Zysler, C.A. Ramos, H. Romero, Magnetization enhancement

at low temperature due to surface ordering in Fe–Ni–B amorphous nanoparticles, Phys. B Condens. Matter. 320 (2002) 203–205. doi:10.1016/S0921-4526(02)00682-8.

[41] R.W. Chantrell, N.S. Walmsley, J. Gore, M. Maylin, Theoretical studies of the field-cooled and zero-field cooled magnetization of interacting fine particles, J. Appl. Phys. 85 (1999) 4340–4342. doi:10.1063/1.370361.

[42] K. Vasundhara, S.N. Achary, S.K. Deshpande, P.D. Babu, S.S. Meena, A.K. Tyagi, Size dependent magnetic and dielectric properties of nano CoFe2O4 prepared by a salt assisted gel-combustion method, J. Appl. Phys. 113 (2013) 194101. doi:10.1063/1.4804946.

[43] A.H. Morrish, The Magnetic Field, Phys. Princ. Magn. (2001) 1–30. doi:10.1109/9780470546581.ch1.

[44] B.D. Cullity, C.D. Graham, Introduction to Magnetic Materials., Wiley, 2011.

[45] C. Vázquez-Vázquez, M.A. López-Quintela, M.C. Buján-Núñez, J. Rivas, Finite size and surface effects on the magnetic properties of cobalt ferrite nanoparticles, J. Nanoparticle Res. 13 (2010) 1663–1676. doi:10.1007/s11051-010-9920-7.

[46] A. Repko, D. Nižňanský, J. Poltierová-Vejpravová, A study of oleic acid-based hydrothermal preparation of CoFe2O4 nanoparticles, J. Nanoparticle Res. 13 (2011) 5021–5031. doi:10.1007/s11051-011-0483-z.

Tables

Table 1. Mössbauer hyperfine parameters at 300 and 4.2K of 57Fe of nanosized $CoFe_2O_4$: A tetrahedral site and B octahedral site (four components:B1-B4). Isomer shift (δ) relative to α-Fe, hyperfine magnetic field (H_{hf}) and relative areas (A).

T		A	B1	B2	B3	B4
300K	δ (mm s^{-1}) $\pm$ 0.002	0.243	0.42	0.39	0.40	0.42
	H_{hf}(T) $\pm$ 0.1	48.9	52.2	50.3	48.3	45.4
	% A $\pm$ 1	39		61		
4.2K	δ (mm s^{-1}) $\pm$ 0.002	0.383	0.49	0.51	0.52	0.33
	H_{hf}(T) $\pm$ 0.1	50.8	55.3	54.6	52.7	52.0
	% A $\pm$ 1	38		62		

Table 2. In-field Mössbauer parameters of Fe located at tetrahedral and octahedral sites of $CoFe_2O_4$: isomer shift (δ) relative to α-Fe, effective magnetic field (H_{eff}), hyperfine magnetic field (H_{hf}), relative areas (A) and canting angle from each site (θ). A 7 T magnetic field was applied parallel to the γ-beam.

T (K)	δ (mm s^{-1}) $\pm$ 0.002		H_{eff} (T) $\pm$ 0.1		H_{hf} (T) $\pm$ 0.1		A_{rel} (%) $\pm$ 1		$\Theta(^0) \pm 10$	
	Fe_A^{3+}	Fe_B^{3+}	Fe_A^{3+}	Fe_B^{3+}	Fe_A^{3+}	Fe_B^{3+}	Fe_A^{3+}	Fe_B^{3+}	Fe_A^{3+}	Fe_B^{3+}
300	0.285	0.507	55.3	45.2	48.5	52.0	36	64	13	15
100	0.398	0.569	56.3	48.4	49.9	54.8	34	66	14	26
10	0.411	0.557	54.3	48.1	48.1	54.0	36	64	27	34
4.2	0.408	0.557	55.4	47.4	49.0	53.5	36	64	23	31

Table 3. Structural data and magnetic moments at 100 ==and== 800 K obtained from neutron powder diffraction patterns shown in Figure 7. ==B is the isotropic Debye-Waller factor for each atoms.==

T(K)	800 K	100 K
a(Å)	8.44749(8)	8.38474(7)
x(O)	0.2555(2)	0.2555 fixed
B (O) (Å^2)	1.42(3)	0.63(3)
B_t (Å^2)	0.84(6)	0.05(4)
B_o (Å^2)	1.36(5)	0.68(6)
Co at 8a	0.0114(4)	0.0114 fixed
Co at 16d	0.0302(4)	0.0302 fixed
Fe at 8a	0.0303(2)	0.0303 fixed
Fe at 16d	0.0531(2)	0.0531 fixed
M_t (μ_B)	0	4.04(8)
M_o (μ_B)	0	3.25(6)
R_B	5.8	4.84 / Magnetic 9.57
R_F	5.12	4.25
χ^2	==2.73==	==2.42==

Table 4. Magnetic parameters obtained from magnetic cycles and M_s approach law at 100, 200 and 300 K.

T(K)	M_S (emu g^{-1})	M_S (μ_B)	K x 10^5 (J m^{-3})	H_C (kOe)	M_r (emu g^{-1})
100	90.2 (6)	3.79(12)	8.04(10)	7870	60.8
200	89.7(1)	3.77(2)	5.48(3)	3353	50.6
300	79.05(8)	3.32(6)	4.56(11)	1125	32.0

Figure Caption

Figure 1. a), b) and c) Cs-corrected STEM-HAADF image of various nanoparticles subjected to analysis. EELS chemical maps, d) extracted O-K map, e) Fe-$L_{3,2}$ map and f) Co-$L_{2,3}$ map.

Figure 2. a) Co K-edge XAS spectra of $CoFe_2O_4$, CoO, Co_3O_4 and Co-foil, and b) Fe K-edge XAS spectra of $CoFe_2O_4$, γ-Fe_2O_3, Fe_3O_4, FeO and Fe-foil. Inset a) pre-edge of Co and inset b) pre-edge of Fe.

Figure 3. a) Modulus of Fourier transforms of k^3-weighted Co K-edge EXAFS signal between 3 and 10 $Å^{-1}$, of $CoFe_2O_4$ sample and CoO and Co_3O_4 references, and b) modulus of Fourier transforms of k^3-weighted Fe K-edge EXAFS signal between 3 and 10 $Å^{-1}$, of $CoFe_2O_4$ sample and γ-Fe_2O_3 and Fe_3O_4 references.

Figure 4. Mössbauer spectra of $CoFe_2O_4$ recorded between 875 and 4.2K. a), b), c) and d) spectra recorded without external magnetic field at different temperatures, e) and f) spectra recorded applying a magnetic field of 7 T parallel to the γ-beam at 300 K and 4.2 K.

Figure 5. Temperature variation at tetrahedral (square) and octahedral sites (circle) of hyperfine magnetic fields in $CoFe_2O_4$. Open symbols correspond to the values obtained when applying an external field of 7 T parallel to the γ-beam.

Figure 6. Thermal evolution of neutron diffraction patterns of $CoFe_2O_4$ at D1B, from 430 to 810 K.

Figure 7. Neutron powder diffraction pattern at a) 800 K and b) 100 K of $CoFe_2O_4$. Open circles are experimental data, red line is the calculated pattern and blue line is the difference between experimental and calculated data. The first line of green marks corresponds to the allowed Bragg reflection for the crystal structure, and the second line to the magnetic structure reflections

Figure 8. Temperature dependence of the experimental magnetic moment obtained by neutron diffraction experiments at tetrahedral (blue square) and octahedral (red cycles) sites and total (black triangle) magnetic moment.

Figure 9. a) ZFC and FC curves of $CoFe_2O_4$ nanoparticles. For the sake of comparison, 0.1 kOe data are multiplied by a factor 4. b) Magnetic hysteresis loops at 100, 200 and 300 K for $CoFe_2O_4$ nanoparticles.
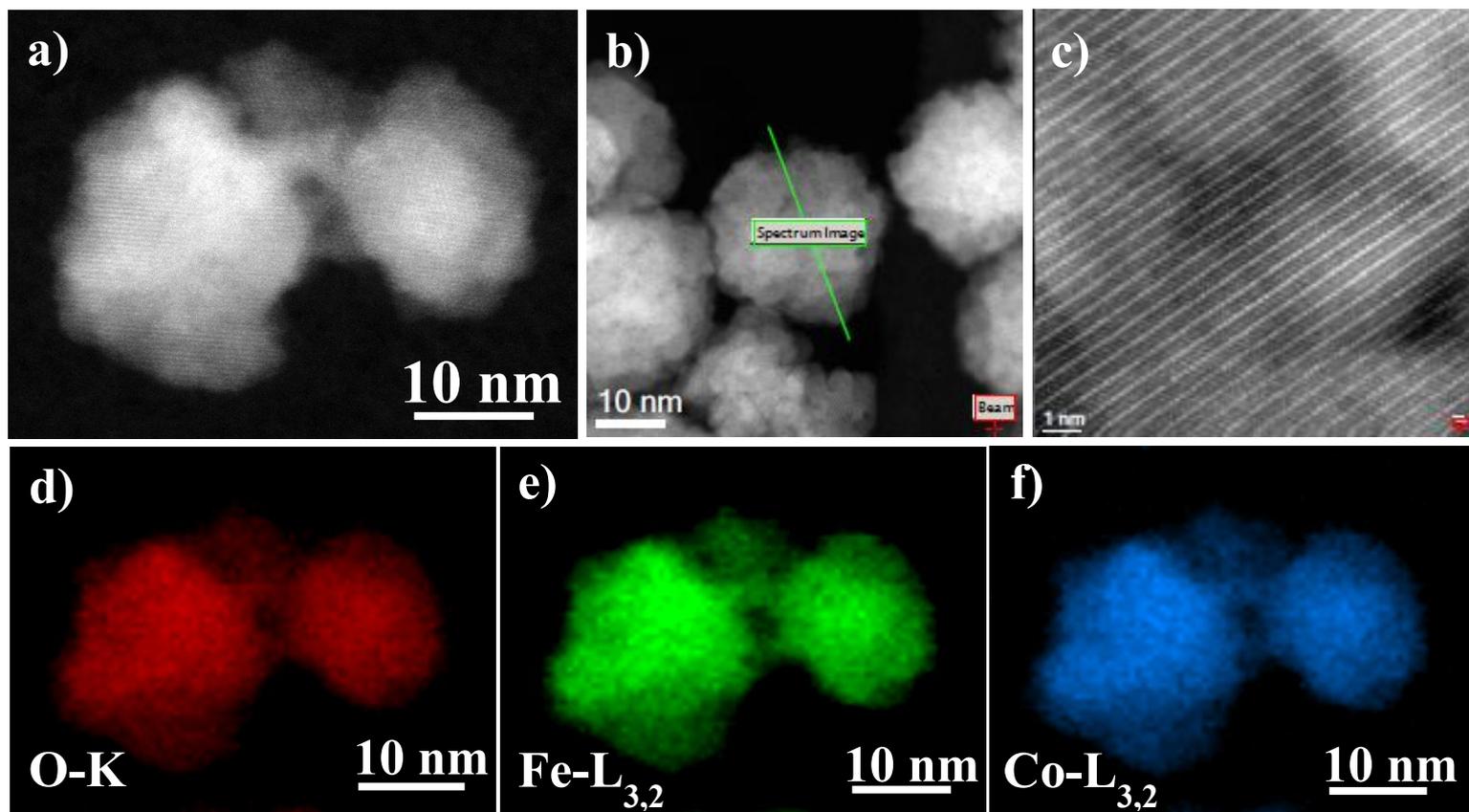
Figure 1
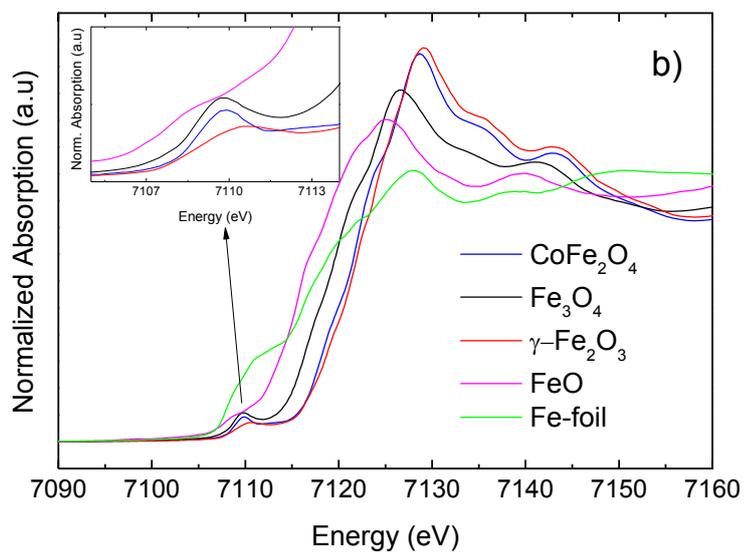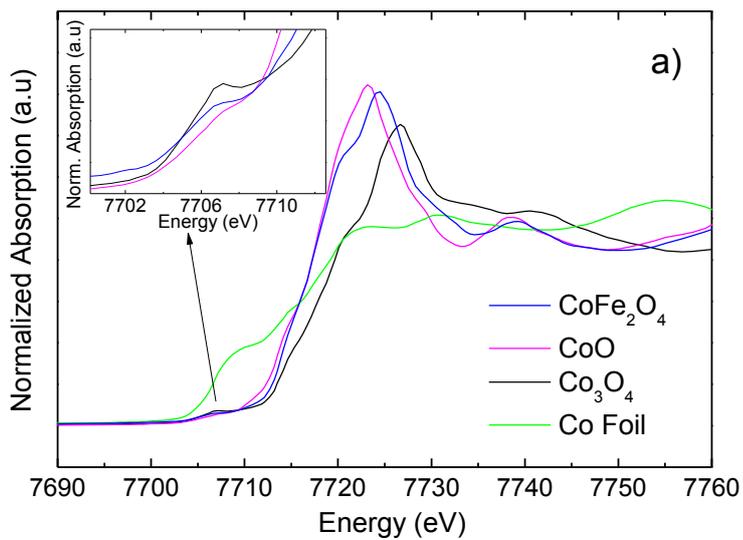
Figure 2
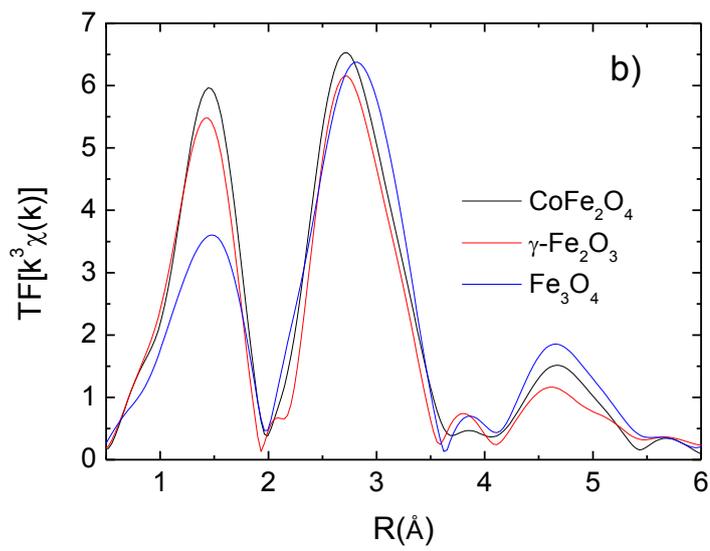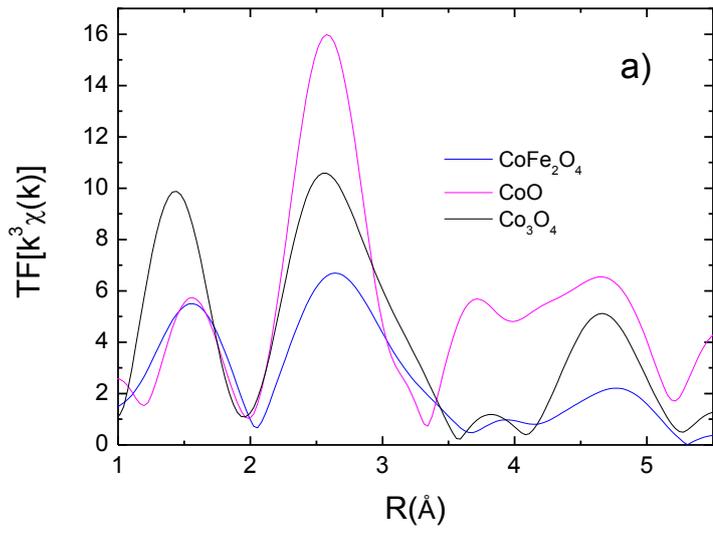
Figure 3
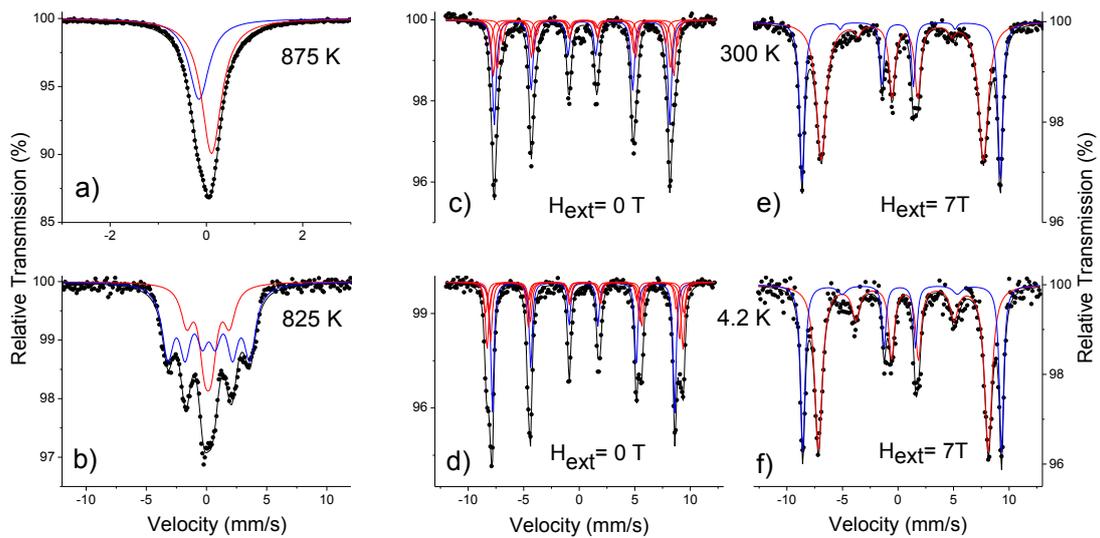
Figure 4
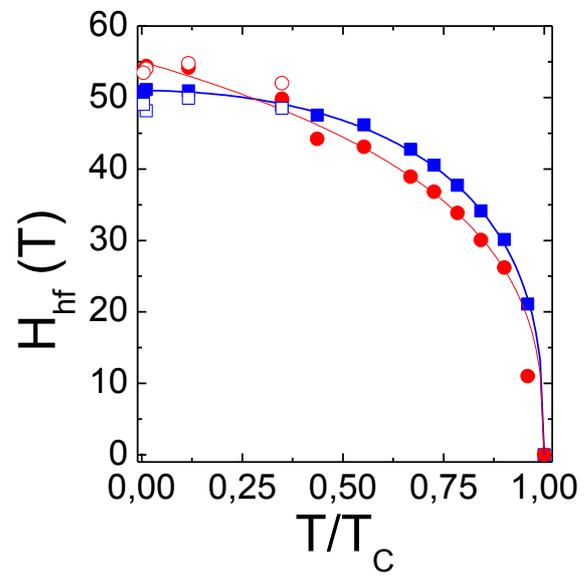
Figure 5
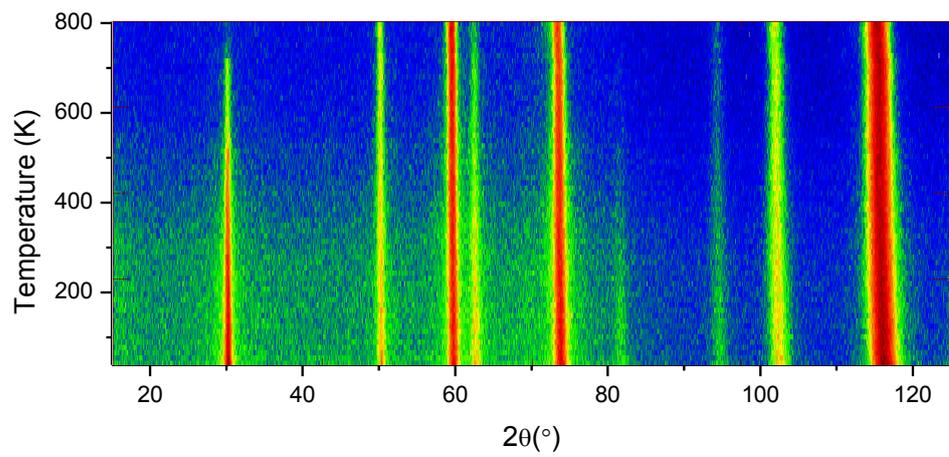
**Figure 6**
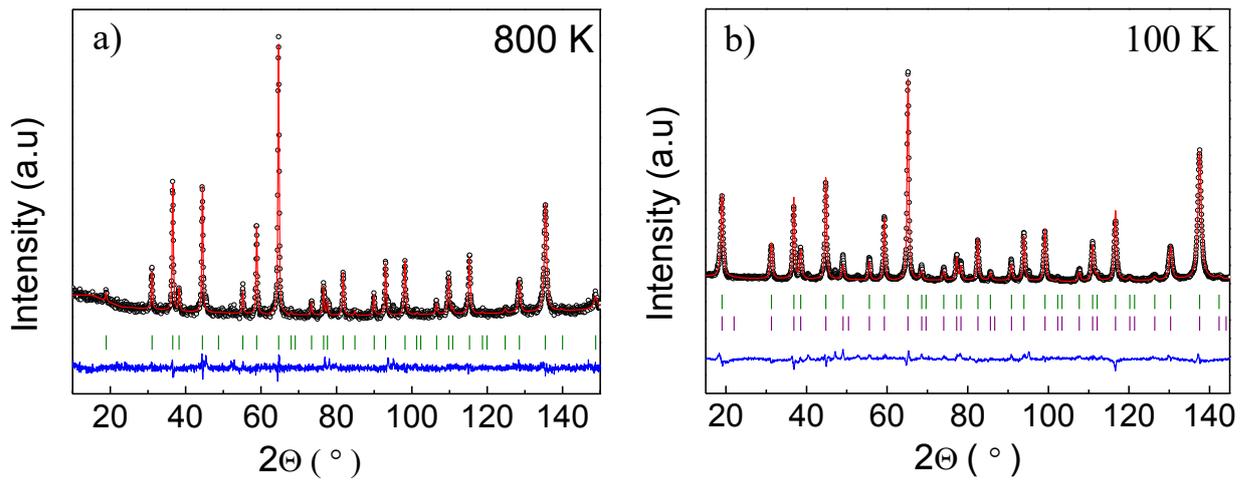
Figure 7
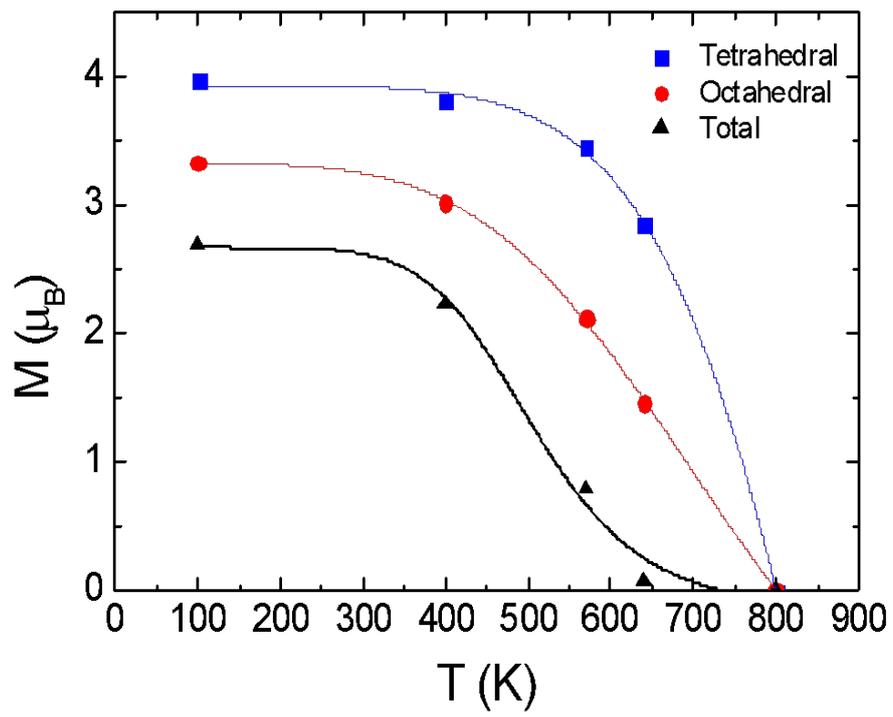
Figure 8
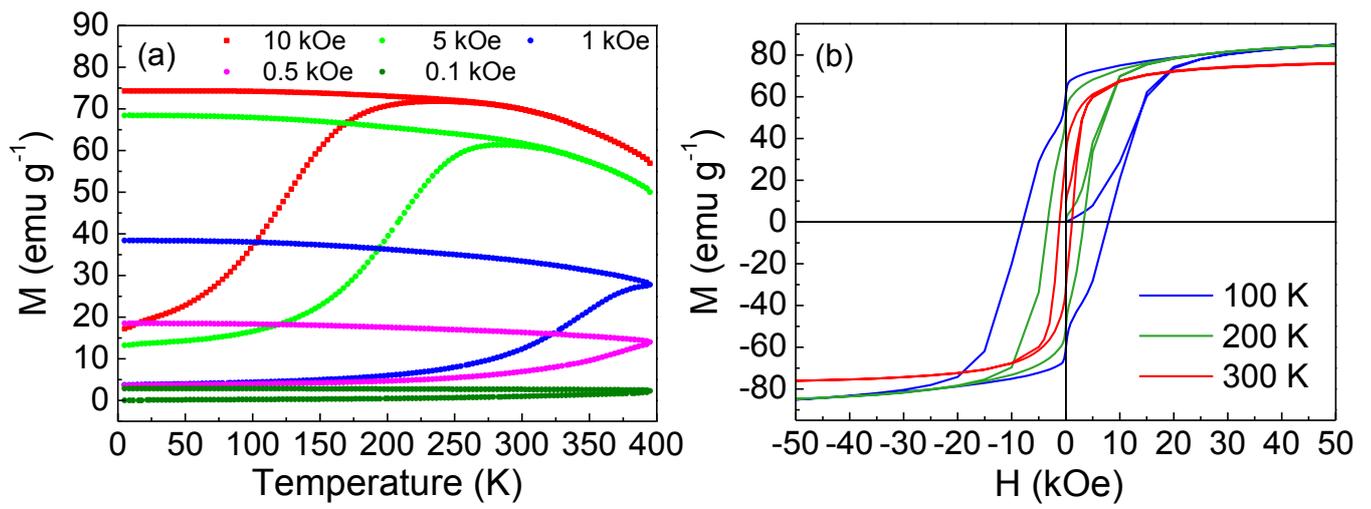
Figure 9

Graphical Abstract
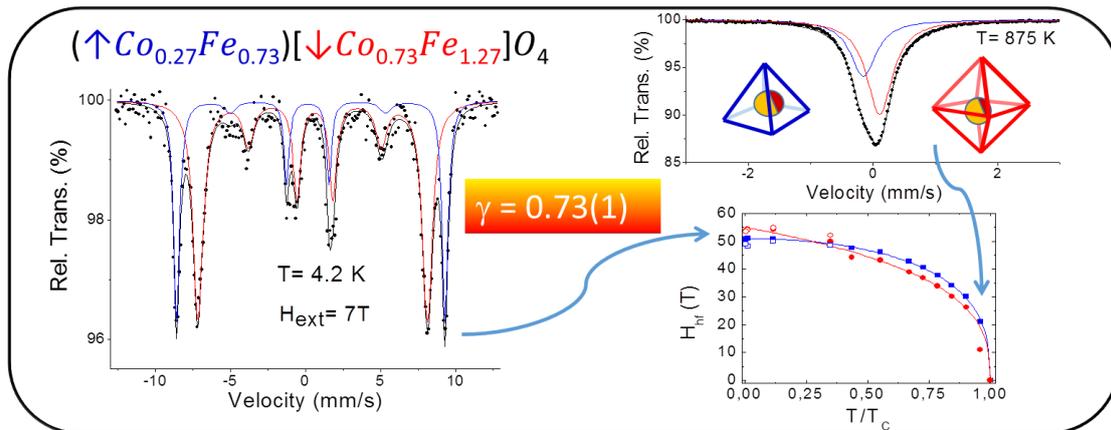
Inversion degree of electrosynthetized cobalt ferrite nanoparticles obtained by neutron diffraction and Mössbauer spectroscopy.

$(\uparrow Co_{0.27}Fe_{0.73})[\downarrow Co_{0.73}Fe_{1.27}]O_4$

$\gamma = 0.73(1)$

T= 4.2 K

H_{ext}= 7T

T= 875 K
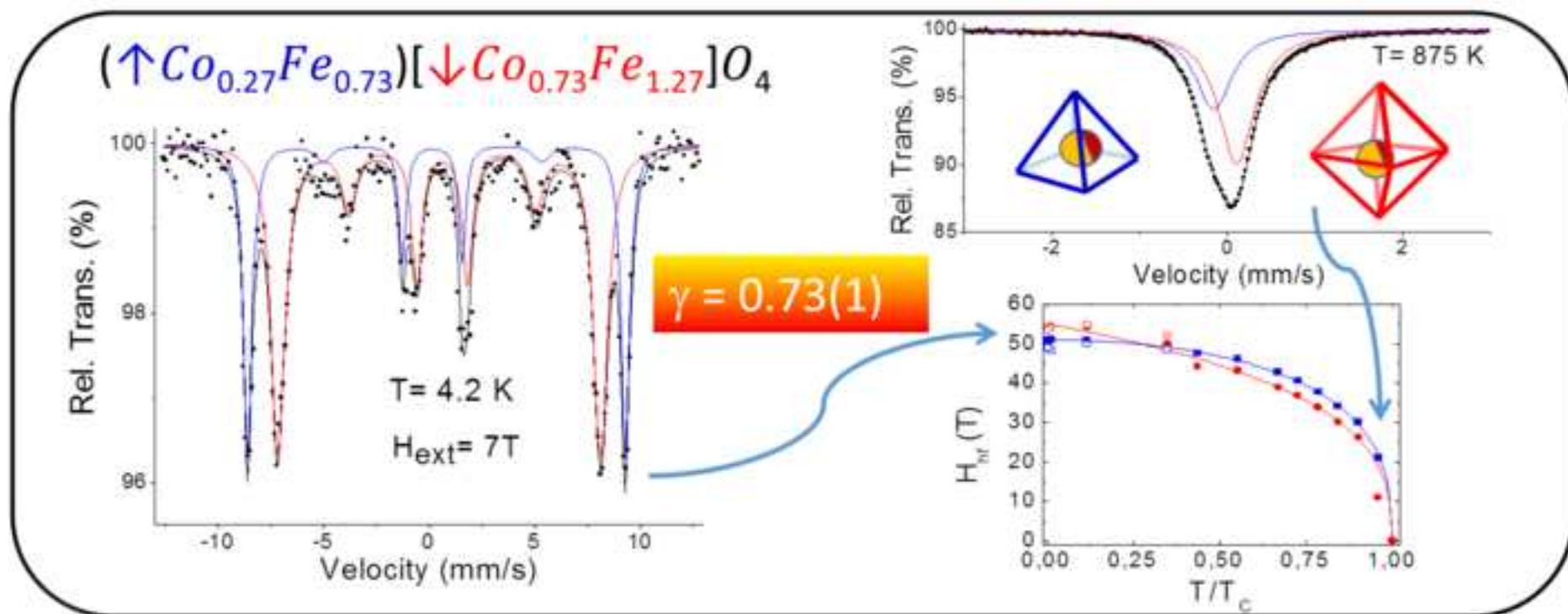
Highlights

- Stoichiometric cobalt ferrite was obtained by electrosynthesis at 25ºC

- Ferrite inversion obtained by X-ray Absortion, Mössbauer and Neutron Difraction.

- A $\gamma=0.73(1)$ is obtained by Mössbauer spectroscopy and neutron diffraction

- Nanoferrites of 22 nm present a crossing of the tetrahedral and octahedral H_{hf}